# Synthesis And Characterization of Mesoporous SBA-15 And SBA-16 Using Agro Waste Such As Rice Husk Ash As Carriers To Improve The Albendazole Dissolution Rate

Dr. Manish Deshpande<sup>1</sup>, Rahul Dasarwar<sup>2</sup>, Amal S. Al- Raboei<sup>3</sup>, Rajesh Bhise<sup>4</sup>, Ameer M. Al-Talqi<sup>5</sup>

<sup>1</sup>Head and Research Supervisor, Dept. Of Physics and Material Science, Netaji Subhashchandra Bose Arts, Commerce and Science College, Nanded, MS India-431601 <sup>2</sup>Research Scholar, Dept. Of Physics and Material Science, Netaji Subhashchandra Bose Arts, Commerce and Science College, Nanded, MS India-431601

<sup>3</sup>Department of Physics, Faculty of Applied Sciences and Humanities, Amran University, Republic of Yemen

<sup>4</sup>Research Scholar, Dept. Of Physics and Material Science, Netaji Subhashchandra Bose Arts, Commerce and Science College, Nanded, MS India-431601

<sup>5</sup>School of Physical Sciences, Swami Ramanand Teerth Marathwada University, Nanded 431606, MS, India

Aim: The aim of this research is to synthesis and characterize mesoporous silica materials derived from Rice husk ash and examine their efficacy as Albendazole carriers, with an emphasis on enhancing dissolving rate.

Methods: Albendazole was impregnated into the mesoporous silica materials SBA- 16 and SBA-15. Particle size distribution, XRD, FT-IR, and scanning electron microscopy to characterize the unloaded and burdened materials were used. Element examination was used to determine the quantity of albendazole in the carriers. The components that were added were tested for their solubility and release properties. The rate of Albendazole dissolution in mesoporous materials was investigated using mathematical models.

Result: Differential scanning calorimetry proved that the adsorbed ABZ was non-crystalline by showing that its dissolution rate was much higher than that of crystalline ABZ. For ABZ/SBA-15, the Weibull model successfully reproduced drug release properties, but for pure Albendazole and ABZ/SBA-16, the Gompertz function worked well. With its rapid drug loading and dissolving rate,

the SBA-15 carrier showed tremendous promise as a material to improve the bioavailability of ABZ.

Conclusion: To Treat hydatidosis more effectively, it is necessary to increase ABZ's water solubility and dissolving rate.

Keywords: Albendazole, Mesoporous, Rice husk ash, Silica, XRD.

#### 1. Introduction

Increased worldwide prevalence of parasitic illnesses demands the development of viable medicinal solutions. Albendazole (ABZ), a broad-spectrum anthelmintic, is extensively used in the treatment of several parasitic illnesses. However, its clinical effectiveness is often constrained by inadequate solubility and diminished bioavailability, which may impede therapeutic results. Innovative drug formulation procedures are required to tackle this difficulty, and the use of mesoporous materials has emerged as a viable solution [1]. When it comes to simple cysts or cysts located in non-essential areas of the body, antiparasitic medications are the better option, especially when the patient is at high risk for surgical intervention [2]. The enhancement of bioavailability and solubility of poorly soluble pharmaceuticals, exemplified by albendazole (ABZ), is a considerable problem in the pharmaceutical sector, especially in light of the increasing incidence of parasitic illnesses globally. Albendazole, a commonly used anthelmintic, is recognized for its effectiveness against several parasitic infections; nevertheless, its therapeutic potential is often constrained by its poor water solubility, resulting in insufficient absorption in the gastrointestinal tract [3-5]. To address this constraint, novel drug delivery strategies are crucial, and mesoporous silica materials have surfaced as a viable possibility. SBA-15 and SBA-16 are distinguished by their elevated surface area, adjustable pore dimensions, and biocompatibility, making them superior options for improving drug dissolving rates.

Conventional synthesis techniques for mesoporous silica often use costly and non-renewable resources, which raises environmental issues and constrains the scalability of these materials. The use of agricultural waste, particularly rice husk ash (RHA), offers a sustainable option [6-8]. Rice husk ash (RHA) is plentiful in silica and constitutes a significant by-product of rice processing [9]. It is an affordable precursor for the synthesis of SBA-15 and 16 and helps with waste valorization when turned into mesoporous silica. Mesoporous silica SBA-15 is characterized by its highly organized hexagonal form and parallel pores. Micropores are formed when the hydrophobic ethylene oxide chain makes its way through the silica walls. Structured by cubically arranged spherical body-centered nanocages, SBA-16 is a kind of mesoporous silica [10-12]. The eight spheres that surround each other are linked. The structural variation may either enhance or diminish the efficiency of processes such as catalysis or separations. Transforming RHA into mesoporous silica enhances medication delivery systems while promoting waste valorization and environmental sustainability. Rice husk (RH) is an important agricultural byproduct that lacks economic use. Processing RH is challenging because to its high content of amorphous silica (15–23 weight percent), which may be present as opal [13, 14]. Consequently, RH is often rejected because to its detrimental impact on the environment. Conversely, the substantial presence of silica transforms RH into a template-containing precursor for the synthesis of porous carbons

[15,16]. The purpose of this research is to synthesis and characterize mesoporous silica materials derived from RHA and examine their efficacy as albendazole carriers, with an emphasis on enhancing dissolving rate [17,18].

This study investigates the characterization and synthesis of mesoporous SBA-15 and 16 using rice husk ash (RHA) as carriers to enhance the solubility rate of albendazole. Following this introduction, the study analyzes the existing literature on mesoporous silica materials, highlighting their structural properties, production methods, and their role in improving drug release profiles. The methods section outlines the experimental procedures for synthesizing SBA-15 and SBA-16, along with the characterization techniques used to assess their structural and textural properties. The results are then presented, including the drug release kinetics and the effectiveness of these mesoporous carriers in enhancing albendazole solubility. The discussion section evaluates the data, explores their implications for pharmaceutical formulations, and recognizes the study's limitations. The study concludes with recommendations for future research, emphasizing the potential for further optimization of these mesoporous materials to improve drug delivery methods for less soluble medications.

# 2. Methodology

#### 2.1 Materials

Rice husk ash (RHA), Pluronic F127, and P123 were purchased from Sigma Aldrich. Crystalline albendazole with a purity level of 98.52% was sourced from Parafarm, while C<sub>4</sub>H-OH, CH3COOH, and HCL acid were acquired from Anedra. The KBr-grade material was purchased from Merck. The reagents were used exactly as they were given and were of analytical grade.

2.2Synthesis of mesoporous silica carriers, Santa Barbara Amorphous-15, and Santa Barbara Amorphous-16

Pluronic P123 was first solubilized in HCL acid solution at 40 degree celsius. After full dissolution, RHA was included, and the medium was kept at 40 degree celsius while being stirred for 2 hours. The gel composition consisted of 1 RHA, 0.017 P123, 5.68 HCl, and 197 H2O. A sealed polypropylene jar was used to conduct hydrothermal synthesis in an oven set at 90 degree celsius for 24 hours. After collecting the solid material using Büchner filtration, it was washed with distilled water and dried in a 70°C oven overnight. The solid was then calcined in a muffle furnace for four hours, heating to 300 °C in air at a rate of one degree Celsius per minute. The following gel composition was used to manufacture SBA-16 according to the approach described by Gobin et al. (2007): 1 thermos, 0.003 fluoroacetic acid, 0.8 hydrochloric acid, 1.8 chloroform, and 120 water. A solution of hydrochloric acid was used to dissolve Pluronic F127. The addition of butanol as a co-surfactant was made after 30 minutes of agitation. After that, TEOS was added and mixed for 24 hours at 25 degrees Celsius [19]. The concoction was subjected to oven heating for 48 hours at 60°C in a Teflon autoclave. Three 30-minute centrifugation cycles at 5000 rpm were used to further purify the material using tridistilled water. The produced material was then dried overnight at 70 degrees Celsius in an oven. After that, the solid was calcined for six hours at 500°C,

two degrees Celsius per minute, in a muffle furnace.

# 2.3Drug loading procedure

ABZ was loaded onto SBA-15 and SBA-16 using the immersion process. In order to do this, 25 milliliter of acetic acid was used to fully dissolve 1250 mg of ABZ. Following that, 419 milligrams of the designated "mesoporous silica particles" were inserted. For 48 hours, the material was kept at room temperature (25°C) with agitation. The sample underwent a 30-minute, 8000 rpm centrifugation to separate the precipitated particles from the supernatant. For the first 72 hours, the materials were desiccated at room temperature.

#### 2.4Characterization

# > X-ray diffraction

The configuration of a crystal may be ascertained by the method of X-ray diffraction (XRD). X-rays possess wavelengths in the angstrom range, exhibit sufficient energy to penetrate materials, and are well suited for investigating their interior structure. It is used to ascertain the bulk phases, degree of crystallinity, unit cell characteristics, and to evaluate particle size. To determine the XRD pattern of a powdered sample, a fixed X-ray source and a movable detector are used. The detector detects the diffracted radiation intensity according to the angle 20 between the incident and diffracted beams. Synthesized catalysts were evaluated using X-ray diffraction utilizing a Rigaku Miniflex-2 goniometer powder diffractometer on finely powdered samples with monochromatic radiation. Under a wavelength of 1.540 Angstrom, the scans were performed with a step size of 0.02 and a step time of 1.2 seconds. XRD patterns were captured for  $2\theta$  values between 2 and 100 for materials with mesopores.

#### Surface area (BET) and Pore size distributions

Adsorbing probing molecules of varied sizes is within the molecular sieve's capabilities. The pore volume, hydrophobicity/ hydrophilicity, and pore widths, of molecular sieves may be inferred from the sorption capacities of probe molecules, which include water, n-hexane, benzene, and nitrogen. The "Brunauer-Emmett-Teller (BET)" volumetric gas adsorption method using nitrogen, argon, and similar gases is the conventional methodology for ascertaining the pore size and surface areas distribution of finely split porous materials. The adsorption isotherm is a metric that illustrates the relationship between the equilibrium pressure of the gas and the quantity adsorbed at a constant temperature. At liquid nitrogen temperatures, nitrogen is frequently employed as an adsorbate. The MCM-41, MCM-48, and SBA-15 N2 adsorption-desorption isotherms illustrate the type IV isotherm characteristic. The substantial increase in N2 adsorption is a sign of capillary condensation within uniform pores.

## > Fourier transform infrared (FTIR) spectroscopy.

Framework infrared spectroscopy offers further insights into the structural characteristics of molecular sieves. It may be used to verify acidity and isomorphic substitution in molecular sieves. The IR spectrum between 200-1300 cm-1 is used to characterize and distinguish the framework architectures of various molecular sieves. Isomorphous replacement of metal ions, such as B, Fe, and Ga for Al, and Ge, V, and Ti for Si, also results in a change in band positions. A supplementary band at 960 cm-1 may be seen in Ti or V substituted molecular

sieves. The infrared bands between 3600-3700 cm-1 validate the existence of silanol or bridging hydroxyl groups in the molecular sieves, allowing for a comparison of their Bronsted acidities.

#### > Scanning electron microscopy:

SEM is a popular technique that provides information on the topography and chemical makeup of catalysts by analyzing their size and shape. Scanning Electron Microscopy (SEM) generates enlarged pictures using electrons rather than light waves. It displays very detailed three-dimensional pictures at much greater magnifications and elemental composition mapping. The crystallite shape and size of the synthesized and calcined samples were assessed using a SEM with energy dispersive X-ray analysis (EDAX) capabilities.

#### > TPD of ammonia:

In the TPD approach, fundamental, volatile probe molecules such as NH3, pyridine, quinoline, or n-butylamine are first permitted to adsorb onto an active solid catalyst at a specified temperature. The adsorbed molecules are then let to desorb in a flow of N2 or Ar by systematically heating the catalyst material. The quantity of ammonia desorbed from the catalyst was assessed using temperature-programmed desorption at the reactor exit. The TPD curves may be deconvoluted into distinct peaks, and the regions under these peaks are translated into milliequivalents of NH3 per gram of catalyst, based on the injection of known quantities of NH3 under comparable circumstances. Using chromatographic techniques, researchers investigated the synthesized sample's temperature-programmed desorption. A flame ionization detector was used to collect the data by use of a Perkin Elmer Sigma 3B gas chromatograph. A flow rate of 40 cc/min of nitrogen was used as the carrier gas.

## > Energy Dispersive Analysis of X-ray:

In EDAX examination, the specimen undergoes bombarded by an electron beam. The accelerated electrons collide with the specimen's electrons, resulting in the displacement of some. An inner shell electron's expulsion creates a void that is subsequently filled by a higher-energy electron from an outer shell. The outer electron being transferred must dissipate a part of its energy by emitting an X-ray. The energy produced by the transferring electron is contingent upon the originating shell and the destination shell involved in the transfer. Moreover, the atom of each element emits X-rays with distinct energy levels throughout the transfer process. The EDX examinations of calcined materials were conducted using Kevex equipment in conjunction with a Jeol JSM-5200 scanning microscope.

#### ➤ Gas Chromatography Mass Spectrometry:

The catalytic efficacy of the pre- and post-modified SBA-15 and SBA-16 catalysts presented in this thesis has been evaluated for many reactions. The conversion, yield, and selectivity were determined using the GC findings. The materials were evaluated using gas chromatography (Shimadzu-2025). The elemental analysis of the resultant product was conducted using a Shimadzu Instruments AA6200 elemental analyzer from Japan.

## ➤ Differential scanning calorimetry

To ascertain the physical states of the drug and its modified mesoporous silica samples, a *Nanotechnology Perceptions* Vol. 20 No.6 (2024)

differential scanning calorimetry investigation was conducted. Thermograms of each sample were obtained with a steady flow of nitrogen gas at a rate of 10 milliliter per minute and a temperature gradient ranging from 25 to 260 degrees Celsius.

# Solubility studies

The three sealed flasks containing 2 milligram per milliliter of Albendazole were used to manufacture the pure drug, which is 25 times more than the drug's solubility as measured in 5 mL of 0.1 N HCl solutions at 37 degrees Celsius. Both the "ABZ/SBA-15 and ABZ/SBA-16" were tested for Albendazole solubility using the loaded materials with the same quantity of drug content. To dissolve the powders, 5 milliliters of a solution containing 0.1 N HCl was heated to 37 degrees Celsius. After four days of constant shaking, the samples had reached solubility equilibrium. After passing through a 0.45 micrometer membrane filter, the samples were analyzed spectrophotometrically at 290 nanometers, which is the highest absorption wavelength of Albendazole in 0.1 N HCl, using a T60U spectrophotometer.

## ➤ ABZ rate dissolution in SBA-15 and 16

Under sink circumstances, a dissolution apparatus II was used to analyze the rate of ABZ dissolution from "SBA-15 and SBA-16" compared to pure Albendazole. At 37°C and 100 rpm, a dissolving medium of 900 mL volume of 0.1 N HCl was used. The concentrations of "ABZ, ABZ/SBA-15, and ABZ/SBA-16" in each dissolving vessel were about 10.0 mg, 33.0 mg, and 78.2 mg, respectively. It was found that the number of Albendazole-loaded carriers could encapsulate about 10 milligrams of ABZ for the purpose of comparison. The following steps were taken to ensure a constant volume: 5 milliliter samples were taken at predetermined intervals, and fresh medium was added at 37°C degrees Celsius using an Agilent 8000 Dissolution Sampling Station. Using a UV-visible spectrophotometer at 290 nanometers, the concentration of ABZ was measured.

## > Drug release kinetic models

Equations (1), (2), (3), and (4) of the "Probit, Gompertz, Weibull, and logistic models" were used to study the release kinetics of Albendazole and carriers loaded with ABZ.

$$\begin{split} F &= F_{max} \, \Phi(\alpha + \beta logt) . & 1 \\ F &= F_{max} e^{-\alpha e(-\beta logt)} . & . 2 \\ F &= F_{max} [1 - e^{-(\alpha \beta/\alpha)}] . . & . 3 \\ F &= F_{max} [e^{(\alpha + \beta logt)}/1 + e^{(\alpha + \beta logt)}] . . . . 4 \end{split}$$

F stands for the maximum fraction of the medicine released at an infinite amount of time, and t is the time at which the medication was released (%). A represents the temporal scale of the process and is used as the scale parameter in all models. The disintegration rate per unit of time is represented by the letter b, which also serves as its acceleration parameter. In Equation (1), T represents the dissolution profile's ordinary normal distribution. The parameters of Equation (1) were calibrated by "minimizing the sum of squared errors between experimental data and drug release fractions computed from the cumulative distribution function, whilst the kinetic parameters of Equations (2-4) were determined after linearization". Using the DDSolver software, the accuracy of the obtained parameters was

verified. The effectiveness of the release models that were used in this study to describe the dissolution patterns was evaluated using the Akaike Information Criterion (AIC). The formula (5) defines the AIC:

$$AIC = nln(WSSR) + 2p......5$$

"n indicates the number of dissolution measurements, p refers to the number of parameters modified in each model, and WSSR represents the weighted sum of squared residuals." A reduced AIC score indicates a better fit when evaluating mathematical models.

#### 3 Result and Discussion

3.1 Characterization of Santa Barbara Amorphous -15 and Santa Barbara Amorphous -16

#### 3.1.1X-ray

This is the X-ray of Santa Barbara Amorphous -15, as seen in Figure 1a. The synthesized sample exhibited a well-resolved pattern in the XRD data, with a significant peak at  $2\theta$  about  $0.9^{\circ}$  and two peaks at  $2\theta$  at 1.64 and  $1.8^{\circ}$ . The corresponding "d-spacings are (100) = 9.8 nm, (110) = 5.42 nm, and (210) = 4.9 nm". This symmetrical group is characterized by these planes.

Figure 1b shows the X-ray of SBA-16, which shows its cubic cage structure in three dimensions, belonging to the Im3m space group. Consistent with the data provided in literature, this pattern displays a tiny peak at  $2\theta$  ca.  $1.1^{\circ}$  and a very large peak at  $2\theta$  ca.  $0.78^{\circ}$ . The d-spacings that correspond to (110) are 11.3 nm and (220) is 8.03 nm. The unit cell characteristics of other SBA-16 materials with informed patterns are comparable.

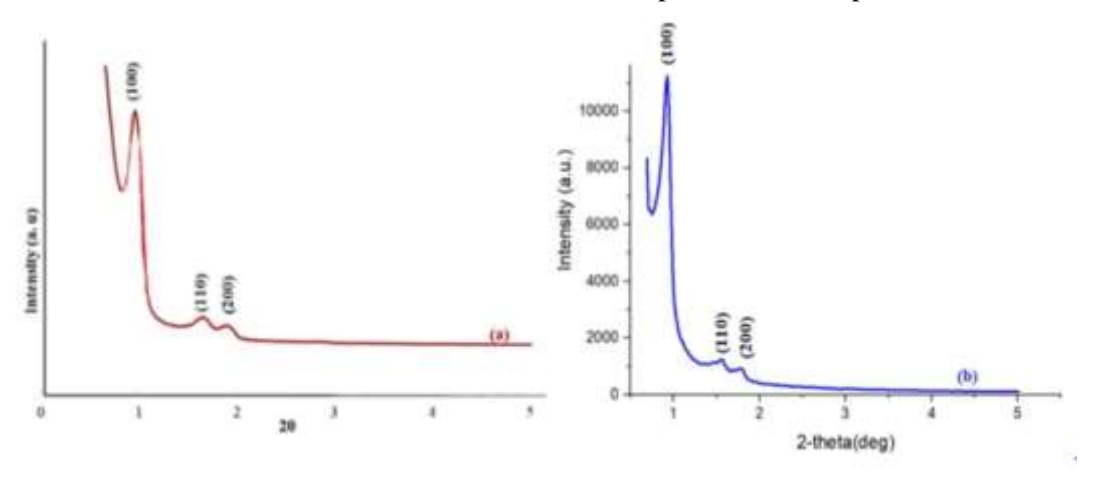


Figure 1. XRD diffraction patterns of: (a) SBA-15 and (b) SBA-16

## 3.1.2Particles' size, pore, and morphology structure

The SEM pictures revealed that SBA-15 particles had a rod-like morphology with a consistent length of around 0.5-1.5 µm. The greatest Feret diameter of Santa Barbara Amorphous -16 particles ranged from 5 to 10 micrometer. Conversely, the observed

morphology aligned with that documented by Belmoujahid et al. (2015)[20]. The majority of Santa Barbara Amorphous -16 particles had an irregular morphology similar to that reported by Feliczak-Guzik et al. (2016) [21].

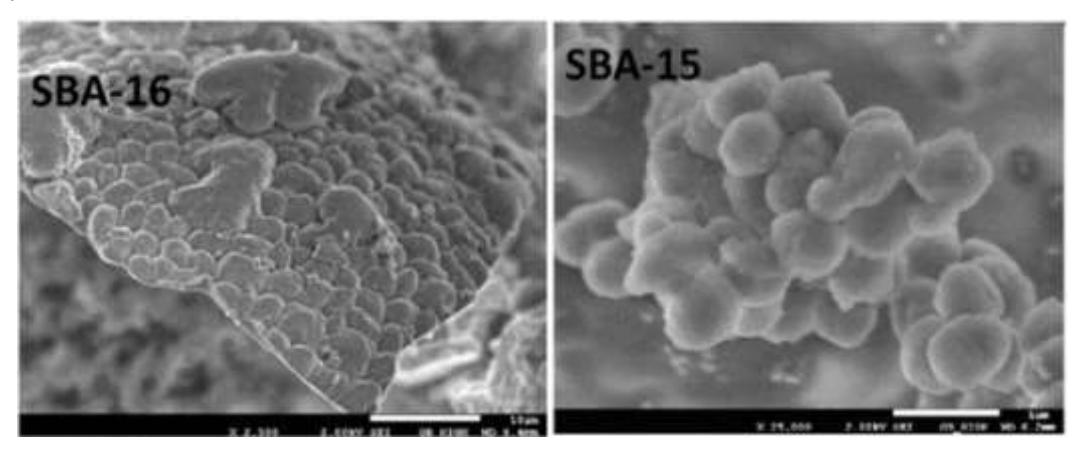


Figure 2. SEM images: (a) SBA-15 and (b) SBA-16

TEM was used to validate the organized pore architecture of SBA-15 and 16. The materials showed notable porosity, according to the microphotographs. When the electron beam was oriented perpendicular to SBA-15's principal axis, a consistently arranged hexagonal array was seen. Image analysis revealed that the average pore width of SBA-15 is around 5 nanometers. Discoveries validated the material's traditional two-dimensional configuration. The typical pore size of SBA-16 was around 6 nanometers, as determined from the photos [22].

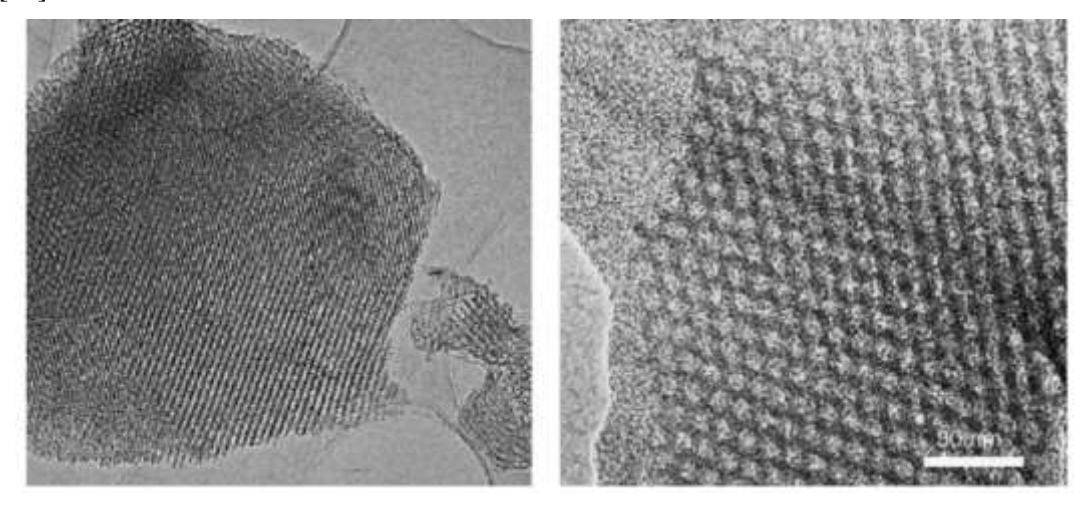


Figure 3. TEM images of (a) SBA-15 and (b) SBA-16

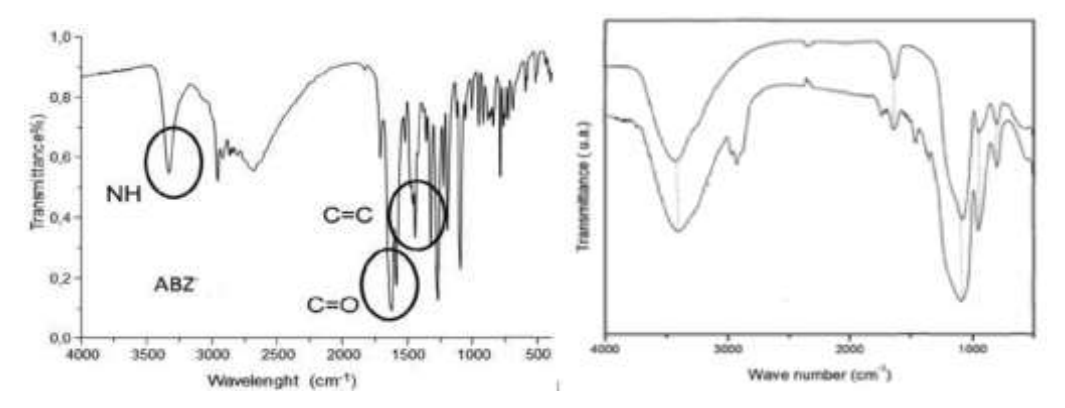
3.1.3FTIR and N2 sorption examinations of the materials Santa Barbara Amorphous -15 and 16 both before and after the addition of Albendazole

The FTIR spectroscopy of pure ABZ is shown in Figure 3a. Around 3323 cm-1, the absorption peak associated with the amide N-H stretching vibration mode was detected. At *Nanotechnology Perceptions* Vol. 20 No.6 (2024)

around 2960 cm-1, the aliphatic hydrocarbon group's absorption band was found. The existence of the RCOOR C=O bond in the carbamate portion of the medicine was revealed by the signal at about 1713 cm-1. The aromatic C=C link and the NH2 N-H bond together make up the benzimidazole portion of the Albendazole molecule, and their peak at about 1623 per cenitmeter corresponds to them. Around 1523 cm<sup>-1</sup>, the band displayed the C=N group's stretching vibration mode. The chemical makeup of the Santa Barbara Amorphous -15 and 16 carriers was further confirmed by the FT-IR spectra (Figure 4b). The Oxygen-hydrogen bond linked to silanol (Si-OH) groups displayed its symmetrical stretching vibration mode in an absorption band located approximately at 3739 cm-1. Water molecules adsorbed on the material's surface exhibit O-H bending and stretching vibrational modes, which are represented by two significant peaks: one at 1630 cm-1 and the other between 3500 and 3300 cm-1. In "SBA-15 and SBA-16", the peak associated with the internal vibration of "Si-O-Si" tetrahedra was located at around 460 per centimeter. The unique band associated with the stretching vibration of the Si-OH group was seen at 970 per centimeter [23,24].

The distinctive band of SBA15 and SBA-16 (at 1080 cm-1) was still visible in the FT-IR spectra after drug loading, suggesting that the materials' surface chemistry had not changed.

Furthermore, FT-IR spectroscopy was used to determine the incorporation of Albendazole in the mesoporous carriers. The following wavenumbers were found to be related with "ABZ in ABZ/SBA-15: 3323 cm-1 (N-H), 2940 cm-1 (C-H), 1712 cm-1 (C=O), 1625 cm-1 (C=C), and 1523 cm-1 (C=N)". The presence of Albendazole within the mesoporous silica was established by the Albendazole/Santa Barbara Amorphous-16 sample. Although the ABZ-associated peak at 3323 per centimeter was not seen, a peak at 1713 per centimeter appeared with an intensity similar to the ABZ/SBA-15 spectrum. The intensity of the bands at around 1623 and 1523 per centimeter was lower than that of the same bands seen in the ABZ/SBA-15 spectra. The results suggest that, in comparison to SBA-15, less ABZ was included in SBA-16. Sorption isotherms and elemental analysis were then used to verify the results [25].



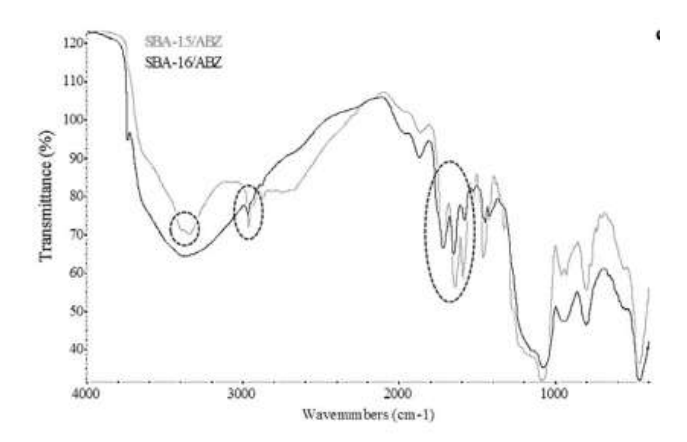


Figure 4. FT-IR spectra of (a) ABZ, (b) SBA-15 and SBA-16, and (c) SBA-15/ABZ and SBA-16/ABZ

The pore size distributions and N2 desorption /adsorption isotherms for "SBA-15, ABZ/SBA-15, 16, and ABZ/SBA-16" are shown in Figure 4. Materials with mesopores and cylindrical channels that are open at both ends in one dimension often exhibit an H1 hysteresis loop, as seen in the SBA-15 isotherm. A homogenous cage-like mesoporous material with linked pores was indicated by SBA16's depiction of an H2 hysteresis loop in the high relative pressure region.

Based on the N2 sorption isotherms of "SBA-15 and SBA-16" after ABZ loading, the reduced total volume of adsorbed N2, indicating that the mesoporous carriers had their pores filled to a large extent. Compared to SBA-16/ABZ, the pore size decrease in SBA-15/ABZ was much stronger. The fact that the isotherm shape was the same after drug loading indicates that the carriers' mesoporous structure was maintained even if their surface area changed. Results for "SBA-15 and SBA-16" in terms of BET surface area were quite close to one another. In comparison to SBA-15, the "total pore volume" of Santa Barbara Amorphous -16 is significantly higher.

Mesoporous silica may provide information on the alterations if ABZ is introduced into its pores. The findings are consistent with those of the "FT-IR and N2 sorption" experiments, which supported the drug's absorption into the materials. Therefore, elemental analysis was used to quantify the drug loading in the mesoporous carriers [26].

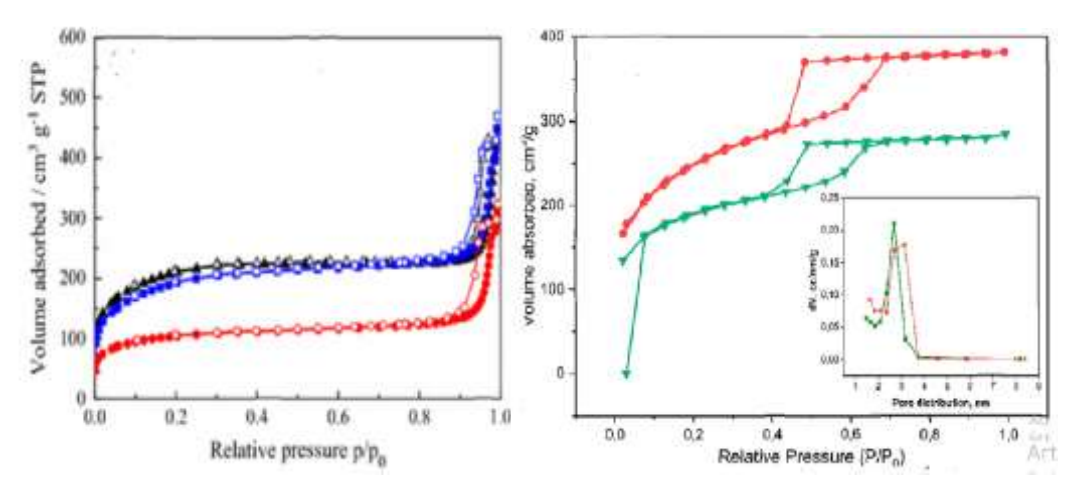


Figure 5. Nitrogen sorption isotherms and pore size distribution (inset) of: (a) SBA-15 and ABZ/SBA-15 and (b) SBA-16 and ABZ/SBA

# 3.1.4Dissolution and Solubility studies

The examination of solubility showed that in an acidic solution (HCl 0.1 N), clear crystal

Albendazole had a minimum solubility of  $0.0152 \pm 0.0002$  mg/mL. The drug solubility was found to be "0.0171  $\pm$  0.0011 mg/mL for ABZ/SBA-16 and 0.0190  $\pm$  0.0013 mg/mL for ABZ/SBA-15, respectively", when ABZ was added to mesoporous materials, compared to pure ABZ. Within the pores, the drug molecules were trapped and retained in situ while they were in their amorphous condition [27].

Table 1 Textural properties						
Sample	SBETa (meter square /gram)	Vt b (gram per cubic centimetre)	Smc (meter square /gram)	Vmd (gram per cubic centimetre)		
SBA-15	382	0.632	33	0.012		
SBA-16	401	0.363	101	0.042		
ABZ per SBA-15	155	0.285	-	0.000		
ABZ per SBA-16	220	0.212	24	0.0 10		

Crystalline solids possess significant crystal packing energy that is compromised during the process of solubilization. Amorphous materials, on the other hand, do not exhibit any long-range molecular order and possess a low packing energy. These features result in pharmaceuticals in an amorphous form often exhibiting superior solubility compared to crystalline substances.

Table 2 Albendazole, Albendazole/Santa Barbara Amorphous -15 and 16 kinetics parameters						
Model	Statistics	Albendazole	Albendazole /Santa Barbara Amorphous-15	Albendazole /Santa Barbara Amorphous-16		
Weibull	α	627.10	3.01	3.22		
	β	1.84	0.50	0.82		

	coefficient of determination	1.00	1.0	1.0
	Akaike Information Criterion	16.43	1.18	11.90
Gompertz	α	25.52	1.73	3.83
	β	2.8	1.03	3.22
	coefficient of determination	1.0	1.0	1.0
	Akaike Information Criterion	10.42	4.12	6.52
Logistic	α	-7.41	-1.22	-1.83
	β	4.90	1.58	3.65
	coefficient of determination	1.00	1.0	1.0
	Akaike Information Criterion	13.02	1.82	6.92
Probit	α	-4.12	-0.77	-1.04
	β	2.80	1.03	2.12
	coefficient of determination	1.0	1.0	1.0
	Akaike Information Criterion	11.92	1.95	8.74

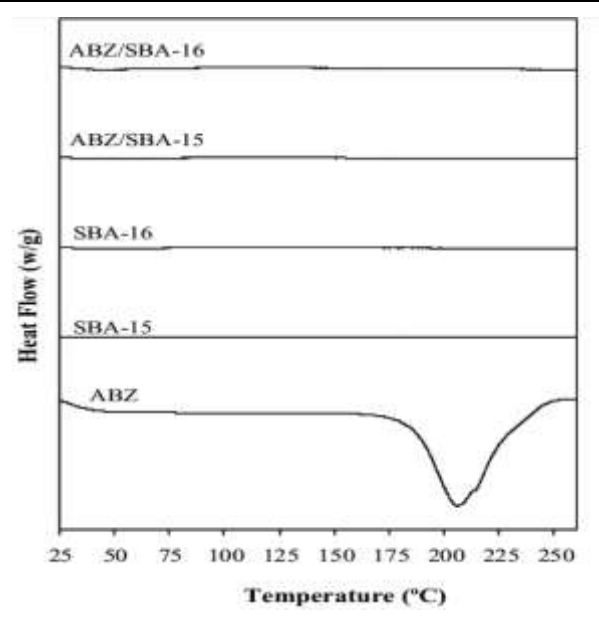


Figure 6. DSC patterns of ABZ, SBA-15, SBA-16, ABZ/SBA-15 and ABZ/SBA-16

Figure 6 unequivocally shows that the "ABZ/SBA-15" and "ABZ/SBA-16" samples' thermograms do not show the crystalline albendazole's melting endothermic peak at 209 degree celsius, showing that the medication is amorphous. The findings indicate that the two mesoporous materials had comparable pore sizes and surface areas. It is possible that the superior solubility of ABZ per SBA-15 is due to its greater total pore volume compared to SBA-16 (Table 1). The extensive number of holes initially enhanced the absorption of the medication, hence improving its interaction with the medium, resulting in increased solubility of the drug [28].

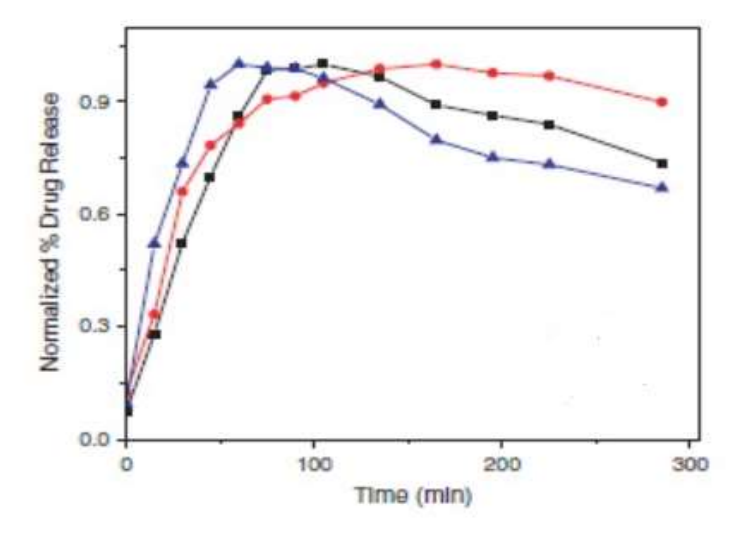


Figure 7. Release profiles of pure ABZ, ABZ/SBA-15 and ABZ/SBA-16.

Figure 7 illustrates a significant increase in the release rate of the encapsulated medication. Specifically, "ABZ/SBA-15 and ABZ/SBA-16" released over fifty percent of the drug at 5 minutes during the experiment, while pure Albendazole released just about 1 percent at the same time interval. SBA-15 demonstrated a release of about 98 ± 2% of the medication within 2 hours, establishing it as a potential option for enhancing the oral bioavailability of ABZ. The superior dissolving rate of "ABZ/SBA-15 relative to ABZ/SBA-16" may be ascribed to its enhanced solubility, coupled with the two-dimensional hexagonal arrangement of the mesopores. The improved ibuprofen release rate of Santa Barbara Amorphous-16 compared to Santa Barbara Amorphous-15 was explained by the change in morphology of the mesoporous materials, as stated by Porras Quevedo et al. (2017). After subjecting SBA-15 to the acidic treatment, its BET surface area rose from 387 to 389-meter square per gram [29]. Researcher found no effect of the acetic acid treatment on SBA-15. El Mourabit et al. (2012) also discovered the same thing when they exposed SBA-15 to phosphoric acid [30].

## 3.1.5Release modeling

To evaluate the ABZ, ABZ per SBA-15, and 16 dissolution profiles, the experimental data was fitted to the logistic, Gompertz, Weibull, and Probit models. The aforementioned data were used to assess the efficacy of the released models. The model Gompertz is the most suitable function for the dissolution data of Albendazole and ABZ per SBA-16, as shown by the coefficient of determination and the Akaike Information Criterion. For ABZ per SSA-15, the Weibull model performs quite well for dissolution data. Medication release profiles with intermediate release rates because the Gompertz model allows one to properly compare Albendazole and ABZ per SVA-16. This model exhibits a rapid initial increase and gradually approaches the asymptotic maximum dissolution [31]. The Weibull model, on the other hand, is more suited to assessing the release patterns of pharmaceuticals contained in carriers, which significantly improves drug dissolution rate. The shape parameter  $\beta$  for ABZ/SBA15 and ABZ/SBA-16 was smaller than 1, indicating that their dissolution profiles had a higher beginning slope than ABZ.

#### 4. Conclusion

The structured, morphological, and textural properties of these mesoporous materials were evident in the synthetic SBA-15 and 16. The solubility of ABZ was enhanced after its amorphous incorporation into the carriers' mesopores. The dissolving rate was significantly increased compared to pure crystalline medicine. Both pure Albendazole and ABZ per SBA-16 have their dissolving properties accurately described by the Gompertz function. The ABZ per SBA-15 is a powder that can be made using simple and potentially scalable procedures. Capsules and other conventional oral pharmaceutical dosage forms are also possible for this drug. To determine if ABZ/SBA15 is an effective therapy for human echinococcosis, more studies evaluating its in-vivo pharmacokinetic effectiveness are required.

#### References

- 1. Abulaihaiti, M., Wu, X., Qiao, L., Lv, H., Zhang, H., 2015. Efficacy of AlbendazoleChitosan Microsphere-based Treatment for Alveolar Echinococcosis in Mice 1– 16. 10.1371/journal.pntd.0003950
- 2. Patel RJ, Patel AA, Patel HP. Stabilized amorphous state of riluzole by immersion-rotavapor method with synthesized mesoporous SBA-15 carrier to augment in-vitro dissolution. Journal of drug delivery science and technology. 2021 Feb 1; 61:102270.
- 3. Belmoujahid Y, Bonne M, Scudeller Y, Schleich D, Grohens Y, Lebeau B. SBA-15 mesoporous silica as a super insulating material. The European Physical Journal Special Topics. 2015 Jul;224(9):1775-85.
- 4. Porras M, Adrover ME, Pedernera M, Bucala V, Gallo L. Novel techniques for drug loading quantification in mesoporous SBA-15 using chemometric-assisted UV and FT-IR data. Journal of Pharmaceutical and Biomedical Analysis. 2022 Jul 15; 216:114830.
- 5. Koohi Moftakhari Esfahani M, Alavi SE, Cabot PJ, Islam N, Izake EL. Application of mesoporous silica nanoparticles in cancer therapy and delivery of repurposed anthelmintics for cancer therapy. Pharmaceutics. 2022 Jul 29;14(8):1579.
- 6. Jittin V, Bahurudeen A, Ajinkya SD. Utilisation of rice husk ash for cleaner production of different construction products. Journal of cleaner production. 2020 Aug 1;263:121578.
- 7. Kumar A, Singha S, Sengupta B, Dasgupta D, Datta S, Mandal T. Intensive insight into the enhanced utilization of rice husk ash: abatement of rice mill wastewater and recovery of silica as a value added product. Ecological Engineering. 2016 Jun 1;91:270-81.
- 8. Nzereogu PU, Omah AD, Ezema FI, Iwuoha EI, Nwanya AC. Silica extraction from rice husk: Comprehensive review and applications. Hybrid Advances. 2023 Nov 21:100111.
- 9. H.S. Mukunda, S. Dasappa, P. J. Paul, N. K. S. Rajan, D.N. Subbukrishna. (2003), A Novel Process and Apparatus for The Manufacture of Precipitated Silica from Rice Husk Ash. Indian Patent No. 216477, 18th Feb 2003
- 10. dos Santos SM, Nogueira KA, de Souza Gama M, Lima JD, da Silva Júnior IJ, de Azevedo DC. Synthesis and characterization of ordered mesoporous silica (SBA-15 and SBA-16) for adsorption of biomolecules. Microporous and Mesoporous Materials. 2013 Nov 1;180:284-92.
- 11. Kim TW, Ryoo R, Gierszal KP, Jaroniec M, Solovyov LA, Sakamoto Y, Terasaki O. Characterization of mesoporous carbons synthesized with SBA-16 silica template. Journal of Materials Chemistry. 2005;15(15):1560-71.
- 12. Mesa M, Sierra L, Guth JL. Contribution to the study of the formation mechanism of mesoporous SBA-15 and SBA-16 type silica particles in aqueous acid solutions. Microporous and mesoporous materials. 2008 Jul 1;112(1-3):338-50.
- 13. Azizi SN, Ghasemi S, Yazdani-Sheldarrei H. Synthesis of mesoporous silica (SBA-16) nanoparticles using silica extracted from stem cane ash and its application in electrocatalytic

- oxidation of methanol. International journal of hydrogen energy. 2013 Sep 30;38(29):12774-85...
- 14. Shelke VR, Bhagade SS, Mandavgane SA. Mesoporous silica from rice husk ash. Bulletin of Chemical Reaction Engineering & Catalysis. 2010 Dec 20;5(2):63-7.
- 15. Silva FE, Rigoti E, Mello MI, Pergher SB. Tuning Textural Properties by Changing the Morphology of SBA-15 Mesoporous Materials. Materials. 2024 Jun 10;17(12):2827.
- 16. Schwanke AJ, Melo DM, Silva AO, Pergher SB. Use of rice husk ash as only source of silica in the formation of mesoporous materials. Cerâmica. 2013; 59:181-5.
- 17. Zhang DD, Hu S, Pan PY, Zhang M, Wu Q, Zhang YR, Zhou XQ. Preparation and antibacterial activity of mesoporous silica based on rice husk ash. LWT. 2023 Aug 1; 185:115145.
- 18. Costa JA, Sarmento VH, Romão LP, Paranhos CM. Adsorption of organic compounds on mesoporous material from rice husk ash (RHA). Biomass Conversion and Biorefinery. 2020 Dec: 10:1105-20.
- 19. Gobin OC, Wan Y, Zhao D, Kleitz F, Kaliaguine S. Mesostructured silica SBA-16 with tailored intrawall porosity part 1: Synthesis and characterization. The Journal of Physical Chemistry C. 2007 Feb 22;111(7):3053-8.
- 20. Belmoujahid Y, Bonne M, Scudeller Y, Schleich D, Grohens Y, Lebeau B. SBA-15 mesoporous silica as a super insulating material. The European Physical Journal Special Topics. 2015 Jul;224(9):1775-85.
- 21. Feliczak-Guzik A, Jadach B, Piotrowska H, Murias M, Lulek J, Nowak I. Synthesis, and characterization of SBA-16 type mesoporous materials containing amine groups. Microporous and Mesoporous Materials. 2016 Jan 15; 220:231-8.
- 22. Q. Li, Z. Wu, B. Tu, S.S. Park, C.-S. Ha, D. Zhao, Microporous and Mesoporous Materials, 135 1094 (2010) 95-104
- 23. H. Zhang, C. Tang, Y. Lv, C. Sun, F. Gao, L. Dong, Y. Chen, J Colloid Interface Sci, 380 (2012) 16-24
- 24. P. Bhange, D.S. Bhange, S. Pradhan, V. Ramaswamy, Applied Catalysis A: General, 400 (2011) 176-184
- 25. Ghosh, B.K., Hazra, S., Naik, B., Ghosh, N.N., 2015. Preparation of Cu nanoparticle loaded SBA-15 and their excellent catalytic activity in reduction of variety of dyes. Powder Technol. 269, 371–378.
- 26. Koradia KD, Parikh RH, Koradia HD. Albendazole nanocrystals: Optimization, spectroscopic, thermal, and anthelmintic studies. Journal of drug delivery science and technology. 2018 Feb 1; 43:369-78.
- 27. Yan H, Zhong X, Liu Y. Improving the Solubility, Stability, and Bioavailability of Albendazole through Synthetic Salts. Molecules. 2024 Jul 29;29(15):3571.
- 28. Lokhandwala H, Deshpande A, Deshpande SH. Kinetic modeling, and dissolution profiles comparison: an overview. Int. J. Pharm. Bio. Sci. 2013 Jan;4(1):728-3.
- 29. Quevedo GP, Celis AC, Ordonez CV, Martinez MO. SBA-type mesoporous materials with cylindrical and spherical structures for the controlled loading and release of ibuprofen. Journal of Sol-Gel Science and Technology. 2018 Feb; 85:486-94.
- 30. El Mourabit, S., Guillot, M., Toquer, G., Cambedouzou, J., Goettmann, F., Grandjean, A., 2012. Stability of mesoporous silica under acidic conditions. RSC Adv. 2, 10916–10924
- 31. Langenbucher F. Letters to the Editor: Linearization of dissolution rate curves by the Weibull distribution. Journal of Pharmacy and Pharmacology. 1972 Dec;24(12):979-81.